bioRxiv preprint doi: https://doi.org/10.1101/312652; this version posted May 2, 2018. The copyright holder for this preprint (which was not certified by peer review) is the author/funder. All rights reserved. No reuse allowed without permission.

Quantification of Enterohemorrhagic *Escherichia coli* O157:H7 proteome using TMT-Based Analysis

Running title: Quantitative EHEC O157:H7 proteome

Wanderson M. Silva[1], Jinlong Bei[2#], Natalia Amigo[1], Pía Valacco[3], Ariel Amadio[4], Qi Zhang[2], Xiuju Wu[2], Ting Yu[2], Mariano Larzabal[2], Zhuang Chen[2], Angel Cataldi[1]*

1 - Institute of Biotechnology, CICVyA, National Institute of Agricultural Technology. Hurlingham, Buenos Aires, Argentina.

2 - AGRO-Biological Gene Research Center, Guangdong Academy of Agricultural Sciences (GDAAS), Guangzhou, China; 4 CEQUIBIEM, FCEN, UBA.

3 - CEQUIBIEM (Mass Spectrometry Facility), IQUIBICEN (Institute of Biological Chemistry Faculty of Exact and Natural Sciences) CONICET (National Research Council-Argentina)

4 - Rafaela Experimental Station, National Institute of Agricultural Technology. Rafaela, Santa Fe, Argentina.

#Co-first author

*Correspondence Author: cataldi.angeladrian@inta.gob.ar

bioRxiv preprint doi: https://doi.org/10.1101/312652; this version posted May 2, 2018. The copyright holder for this preprint (which was not certified by peer review) is the author/funder. All rights reserved. No reuse allowed without permission.

ABSTRACT

Enterohemorrhagic *Escherichia coli* (EHEC) O157:H7 is a human pathogen responsible for diarrhea, hemorrhagic colitis and hemolytic uremic syndrome (HUS). EHEC infection is distributed worldwide and numerous outbreaks of diseases caused by enterohemorrhagic have been reported. To promote a comprehensive insight into the molecular basis of EHEC O157:H7 physiology and pathogenesis, the combined proteome of EHEC O157:H7 strains, Clade 8 and Clade 6 isolated from cattle in Argentina, and the standard EDL933 (clade 3) strain has been analyzed. TMT (Tandem Mass Tags)-based quantitative proteomic and emPAI analyses were performed to estimate the protein abundance in EHEC proteome. 2,234 non-redundant proteins of EHEC O157:H7 were identified. A comparison of this result with *in silico* data of EHEC O157:H7 genome showed that approximately 40% of the predicted proteome of this pathogen were covered. According to the emPAI analysis, 85 proteins were among the most abundant (e.g. GAPDH, FliC H-antigen, Enolase, and GroEL). Tellurite resistance proteins were also highly abundant. COG analysis showed that although most of the identified proteins are related to cellular metabolism, the majority of the most abundant proteins are associated with translation processes. A KEGG enrichment analysis revealed that Glycolysis / Gluconeogenesis was the most significant pathway. On the other hand, the less abundant detected proteins are those related to DNA processes, cell respiration and prophage. Among the proteins that composed the Type III Secretion System, the most abundant protein was EspA. Altogether, the results show a subset of important proteins that contribute to physiology and pathogenicity of EHEC O157:H7.

IMPORTANCE

bioRxiv preprint doi: https://doi.org/10.1101/312652; this version posted May 2, 2018. The copyright holder for this preprint (which was not certified by peer review) is the author/funder. All rights reserved. No reuse allowed without permission.

The study of the abundance of proteins present within a complex mixture of proteins in a cell, under different conditions, can provide important information about the activities of individual protein components and protein networks that are cornerstones for the comprehension of physiological adaptations in response to biological demands promoted by environmental changes. We generated a comprehensive and accurate quantitative list of EHEC O157:H7 proteome, which provides a description of the most abundant proteins produced by this pathogen that were related to physiology and pathogenesis of EHEC. This study provides information and extends the understanding on functional genomics and the biology of this pathogen.

Keywords: EHEC, Tandem mass tags (TMT), protein quantitation, bacterial proteomic

INTRODUCTION

Enterohemorrhagic *Escherichia coli* (EHEC) O157:H7 is a zoonotic pathogen belonging to Shiga toxin-producing *E. coli* (STEC) and responsible for different diseases as diarrhea, hemorrhagic colitis and hemolytic uremic syndrome (HUS). HUS is distributed worldwide and considered to be a public health problem in several countries (1,2). Unfortunately, Argentina is the country with the highest incidence of HUS in the world, with approximately 14 cases per 100,000 in children under 5 and a report of 500 cases per year (3,4). Cattle are the main reservoir of EHEC. Several studies have shown that most cases related to infection in human may be attributed to the high consumption of foods of bovine origin and especially ground beef is the main source of contamination (5).

bioRxiv preprint doi: https://doi.org/10.1101/312652; this version posted May 2, 2018. The copyright holder for this preprint (which was not certified by peer review) is the author/funder. All rights reserved. No reuse allowed without permission.

Great efforts had been made to characterize strains of *E. coli* O157:H7 isolated from Argentinian cattle (6). Using the analysis of simple nucleotide polymorphisms, we have classified 16 strains of STEC O157:H7 in clade 6 and 8, which are the most virulent clades (6). *In vitro* and *in vivo* experimental results showed that the strains Rafaela II (clade 8) and 7.1 Anguil (clade 6) have a high virulence potential when compared with other strains and the standard strain EHEC O157:H7 EDL933 (7). These results enabled us to characterize the high prevalence of strains clade 6 and 8 in the Argentinian cattle. Importantly, these two clades might contribute to a high incidence of SUH in Argentina.

The availability of whole genome sequences of different EHEC strains has enabled genome-wide comparisons to identify factors that might be correlated to physiology and virulence of this pathogen (8). In addition, the implementation of system biology approaches, such as prediction of protein-protein network, has contributed substantially in the understanding of the pathogen and interactions with its host (9).

Information about the functions and activities of the individual proteins and pathways that control these systems is essential to understand complex processes occurring in living cells. Large scale quantitative proteomics is a powerful approach used to understand global proteomic dynamics in a cell, tissue or organism, and has been widely used to study protein profiles in the field of microbiology (10). Furthermore, the study of the abundance of proteins in different conditions or during different stages of growth or disease can provide important information about the activities of individual protein components or protein networks and pathways. The rapid growth of proteomic and genomic methods and tools has managed to reveal the basic protein inventory of a few hundred different organisms. Quantitative proteomic approaches have been applied to

bioRxiv preprint doi: https://doi.org/10.1101/312652; this version posted May 2, 2018. The copyright holder for this preprint (which was not certified by peer review) is the author/funder. All rights reserved. No reuse allowed without permission.

determine the absolute or relative abundance of proteins. This information gives insights about the biological function and properties of the cell as well as how cells respond to environmental or metabolic changes or stresses (11, 12). Quantitative proteomics analysis can contribute to the generation of datasets that are critical for our understanding of global proteins expression and modifications underlying the molecular mechanism of biological processes and disease states.

In a previous study, we reported the use of isobaric tags for comparative quantitation (TMT) method to identify the differentially expressed proteins among three EHEC O157:H7 isolates: Rafaela II (Clade 8), Anguil 7.1 (Clade 6) and EDL933 (Clade 3) (7). The proteome differences observed among these strains are related mainly to proteins involved in both virulence and cellular metabolism; which might reflect the virulence potential of each strain (7). The aim of the present study was to promote a more comprehensive insight into the molecular basis of EHEC O157:H7 physiology and pathogenesis. For this purpose, we applied high-throughput proteomics by performing TMT-based quantitative proteomic analysis and Exponential Modified Protein Abundance Index (emPAI) method (13) to quantify the EHEC O157:H7 proteome.

RESULTS AND DISCUSSION

Global proteomic analysis and functional classification of *Escherichia coli* (EHEC) O157:H7 proteome

The emPAI method was applied to estimate the relative quantification of the EHEC O157:H7 proteome from a dataset generated with strains *E. coli* O157:H7 Rafaela II, Anguil 7.1 and EDL933. The strains were grown in D-MEM media and then, proteins from

bioRxiv preprint doi: https://doi.org/10.1101/312652; this version posted May 2, 2018. The copyright holder for this preprint (which was not certified by peer review) is the author/funder. All rights reserved. No reuse allowed without permission.

total bacterial lysates were extracted and digested in solution. The resulting peptides were labeled with isobaric reagents. Finally samples were pooled and peptides were analyzed by 2D-LC MS/MS.

In our proteomic analysis, we detected 2,519 non-redundant EHEC O157:H7 proteins (**Supplemental material, Table S.1**). When comparing this result with *in silico* data of EHEC O157:H7 genome, approximately 40% of the predicted proteome of this pathogen was identified (**Figure 1A**). To determine the abundance of the identified proteins, emPAI approach (13) was used. Because the emPAI value has a linear correlation with protein concentration, it allows a more accurate estimation of protein abundance. Considering only proteins with at least two peptides per protein, we quantified 2,234 proteins (**Supplemental material, Table S.2**). A dynamic range of protein abundance was generated spanning three orders of magnitude (**Figure 1C**). Eighty-five proteins were identified as most abundant in EHEC O157:H7 proteome (**Table 1)**. Of the 2,234 total proteins, 25 proteins are encoded by genes that are present in the pO157 plasmid; however, these proteins did not show a high abundance level **(Supplemental material, Table S.2)**.

We subsequently performed functional annotation of the identified proteins using gene ontology (14). Cluster of orthologous group (COG) analysis grouped the identified proteins into four important functional groups: (i) metabolism, (ii) information storage and processing, (iii) cellular processes and signaling, and (iv) poorly characterized (**Figure 2A)**. Although most of the identified proteins are related to cellular metabolism, the most abundant proteins are involved in the translation process, followed by energy metabolism

bioRxiv preprint doi: https://doi.org/10.1101/312652; this version posted May 2, 2018. The copyright holder for this preprint (which was not certified by peer review) is the author/funder. All rights reserved. No reuse allowed without permission.

and posttranslational modification, protein turnover and chaperones, which shows an intense metabolic activity mainly in the protein synthesis (**Figure 2B**). On the other hand, most of the less abundant proteins are involved in replication, recombination and repair (**Figure 2B**).

Pieper et al. (15) and Ishihama et al. (16) also conducted proteomic studies on *E. coli* K-12 and EHEC O157:H7 strain 86-24, respectively, to determine the absolute abundance of proteins. Seventy proteins of the most abundant proteins in our study were also found as the most abundant proteins in *E. coli* K-12 **(Table 2)**. Those proteins are related to carbohydrate metabolism, transcription, translation, posttranslational modification and signal transduction mechanisms (16). On the other hand, only 12 proteins of the most abundant group **(Table 2)** were the most abundant ones in the data obtained from quantitative proteome of EHEC O157:H7 strain 86-24 (15). Some of those proteins (e. g. TerD, TerE, EspA and DNA-damage-inducible protein I) are absent from *E. coli* K-12. Interestingly, when comparing our results with those of Pieper et al. (15) and Ishihama et al. (16), the *E. coli* proteome was evaluated in different grown condition. Despite the different growth conditions, glyceraldehyde-3-phosphate dehydrogenase, translation elongation factor Tu, DNA-binding protein H-NS, alkyl hydroperoxidereductase protein C, GroEL chaperone and 50S ribosomal protein L7/L12 were detected as the most abundant proteins as well (**Table 2**). These results suggest a set of proteins that may play an important role in the biology of *E. coli*.

We also detected shiga-toxin subunits such as StxA, StxB, Stx2a and Stx2cb; these proteins, however, were not among the most abundant proteins (**Figure 1**). Pieper et al. (15)

bioRxiv preprint doi: https://doi.org/10.1101/312652; this version posted May 2, 2018. The copyright holder for this preprint (which was not certified by peer review) is the author/funder. All rights reserved. No reuse allowed without permission.

157 also obtained similar results in EHEC 86-24 proteome. This low abundance can be
158 associated with environmental or nutritional conditions that contribute to the bacterial lysis
159 and consequently to the production of the toxin (15, 17, 18).

160 **Metabolic Network Analysis**

161 To identify the most relevant biological pathways of the identified proteins, we performed a
162 KEGG enrichment analysis. This analysis provides a comprehensive understanding about
163 pathways that might contribute to cellular physiology (19). When we evaluated the most
164 abundant proteins, we identified 13 pathways that were considered significant ($p < 0.05$)
165 and the Glycolysis / Gluconeogenesis was the most significant (**Figure 2C**). On the other
166 hand, among the less abundant proteins, we only detected the homologous recombination
167 pathway, which is extremely important for the accurate repair of DNA double-strand breaks
168 (**Figure 2C**). Different studies have reported that glycolysis / gluconeogenesis pathway
169 might influence in the colonization process of EHEC in the gastrointestinal tract of both
170 mouse and bovine (20, 21). Although glycolysis substrates inhibit the expression of genes
171 that are localized in locus of enterocyte effacement (LEE), this pathway plays an important
172 role in the initial colonization and maintenance of EHEC in the mouse intestine. In
173 addition, gluconeogenesis not only induces LEE gene expression, but contributes to the
174 later stages of EHEC colonization in mouse as well (20, 22).

175 In our proteomic analysis, 23 proteins that composed the Glycolysis /
176 Gluconeogenesis pathway of *E. coli* were identified (**Figure 3**). NAD-dependent
177 glyceraldehyde-3-phosphate dehydrogenase (GAPDH) was the most abundant protein of
178 EHEC O157:H7 proteome (**Table 1**). This important cytoplasmic protein of the Glycolysis

bioRxiv preprint doi: https://doi.org/10.1101/312652; this version posted May 2, 2018. The copyright holder for this preprint (which was not certified by peer review) is the author/funder. All rights reserved. No reuse allowed without permission.

pathway is also described as a moonlight protein, owing to the distinct functions performed by this enzyme in different cellular localization (23). Some studies showed that GAPDH secreted by EHEC and enteropathogenic *E. coli* (EPEC) strains can bind to fibrinogen and epithelial cell, which could contribute to the pathogenesis of this bacterium mainly through cell adhesion (24, 25). Another protein that is also described as a moonlight protein and was detected among the most abundant proteins of the EHEC proteome is enolase (**Table 1**) (23). This glycolytic enzyme that plays an important role in the carbon metabolism also acts in the RNA degradosome process, mainly in the RNA processing and gene regulation. In *E. coli*, enolase-RNase E/ degradosome complex regulates bacterial morphology under anaerobic condition by inducing a filamentous form, which is observed by some pathogenic *E. coli* strains under oxygen limiting conditions (26).

Information storage and processing

Most proteins described as the most abundant are involved in translation processes. Similar results had been observed in *E. coli* K-12 (15). In addition, according to the KEGG enrichment analysis, the ribosome was strongly enriched (**Figure 2C)**. We identified proteins involved in structural elements of the ribosome as well as related to initiation, elongation and terminations steps, which are required to the translation process (27). Among these proteins, the translation elongation factor Tu was identified (EF-Tu) (**Table 1**). EF-Tu could play a role in the resistance process of this bacterium in the gastrointestinal tract (28), as well as against cellular damage generated by bile salt sodium deoxycholate (29). These results show an intense metabolic activity of EHEC mainly in protein synthesis. Unlike *E. coli* K-12 (15), the proteins involved in transcription process in EHEC were

bioRxiv preprint doi: https://doi.org/10.1101/312652; this version posted May 2, 2018. The copyright holder for this preprint (which was not certified by peer review) is the author/funder. All rights reserved. No reuse allowed without permission.

identified as most abundant. CspA was identified to be among the most abundant proteins as well. This RNA chaperone is described as the major cold shock protein of *E. coli*. CspA binds to RNA molecules and destabilizes stem loop structures to prevent and resolve misfolding of RNA (30).

Cellular processes and signaling

Flagella are filamentous structures that contribute to pathogenesis of pathogenic *E. coli*, mainly in motility, adhesion and biofilm production (31). Generally, this organelle is constituted by basal body, hook and a filament that is composed by flagelin or flagellar antigen FliC, which belongs to the H-antigens group (31, 32). FliC was detected as highly abundant (**Table 1)**. In addition, a study performed in EPEC showed that FliC might be involved in the inflammatory response during the EPEC infection, due to the capacity of flagelin to induce interleukin-8 (IL-8) release in T84 cells (33).

During infection, *E. coli* is subject to different environmental conditions, for example, temperature changes that occur both in external ambient and within host. In our proteomic analysis, DnaK, GroEL and GroES were detected among the most abundant proteins (**Table 1**). Different studies have shown that these proteins contribute to the resistance process of EHEC under elevated temperature (34, 35). In addition, Kudva et al. (36) demonstrated that DnaK and GroEL were induced when EHEC was grown in bovine rumen fluid, thus showing the contribution of these proteins in the adaptation of EHEC to the bovine rumen.

Other type of stress commonly found by EHEC during the infection process is oxidative stress, which is generated by reactive oxygen species (ROS) such as superoxide

bioRxiv preprint doi: https://doi.org/10.1101/312652; this version posted May 2, 2018. The copyright holder for this preprint (which was not certified by peer review) is the author/funder. All rights reserved. No reuse allowed without permission.

anion (O_2^-) hydrogen peroxide (H_2O_2) and the hydroxyl radical ($OH^·$) produced mainly by host immune response (37). Thus, to adapt and survive under this stress condition, this bacterium presents different anti-oxidant systems. We detected two members of peroxiredoxins (Prxs) family: periplasmic thiol peroxidase (Tpx) and alkyl hydroperoxide reductase C (AhpC) system (**Table 1**). These two antioxidant systems play an important role in the scavengers of H_2O_2 and organic hydroperoxides (38, 39). Glutaredoxin 3 (Grx3) was also among the most abundant proteins (**Table 1**). Grx3 is associated with Glutaredoxin (Grx) system, whose function is to reduce disulfide bond in target proteins to control the intracellular redox environment (40). In addition, Smirnova et al. (41) showed that glutaredoxin proteins might be involved in the resistance of *E. coli* to antibiotics as ampicillin. Altogether, these different systems promote an efficient pathway of antioxidant defense in EHEC that contributes to the pathogenesis of this bacterium.

The *ter* operon related to tellurite resistance is widely spread in several Gram positive and Gram negative pathogenic species (42, 43 In EDL933, this operon is composed by six genes (*terZABCDE*). Among the proteins expressed by that operon, only TerC was absent from our proteomic analysis. Interestingly, TerD and TerE proteins were among the most abundant proteins of EHEC O157:H7 proteome (**Table 1**). A study performed with Uropathogenic *E. coli* (UPEC) isolates showed that the introduction of the *ter* gene cluster contributes to improve bacterial fitness inside macrophages (44). On the other hand, Yin et al. (45) demonstrated that *ter* genes contribute to adherence of EHEC O157:H7 to epithelial cells. However, the true role of these genes in the EHEC pathogenesis remains unclear. Although tellurium is absent from the EHEC niche, interestingly, proteomic studies have detected tellurium resistance proteins in EHEC

bioRxiv preprint doi: https://doi.org/10.1101/312652; this version posted May 2, 2018. The copyright holder for this preprint (which was not certified by peer review) is the author/funder. All rights reserved. No reuse allowed without permission.

O157 proteome in different media and growth conditions such as D-MEM (46), minimal medium (47), CHROMagar™STEC (48), bovine fluid rumen (36) and under conditions that stimulate the quorum sense pathway (49). Despite the several studies in this area, more efforts are necessary to unveil the true role of the tellurium resistance proteins in EHEC pathogenesis.

Locus of Enterocyte Effacement (LEE)

The LEE is a pathogenicity island of 35.6 kb that is organized into five polycistronic operons (*LEE1* to *LEE5*) and is an additional bicistronic operon of glr regulatory proteins (50, 51). LEE is related to intimate adherence of EHEC to cell host and is required for attaching and effacing (A/E) lesions, followed by the translocation of effector proteins that contribute mainly to host modulation of the immune system (52). In addition, LEE contains the genes that encode the Type III secretion system (T3SS) as well as some effectors molecules that are exported by this system. The T3SS is responsible for the translocation of effectors from within the host cell, whose are directly involved in the EHEC pathogenesis, mainly in the host modulation of the immune system (52). In this study the EHEC strains were grown in D-MEM, a medium known to induce expression of genes encoding T3SS (54). We identified 19 LEE-encoded proteins (**Figure 1C, Supplemental material, Table S.2**). Among these proteins, the most abundant were EspA (filamentous structure of the T3SS), EspB (pore formation and effector activity), Tir (translocated intimin receptor) and Intimin (outer membrane adhesin) (**Figure 1C**).

Interestingly, these proteins play an important role in the *E. coli* O157 adhesion (54, 55). On the other hand, EspA, EspB, Tir and Intimin are potential vaccine candidates

bioRxiv preprint doi: https://doi.org/10.1101/312652; this version posted May 2, 2018. The copyright holder for this preprint (which was not certified by peer review) is the author/funder. All rights reserved. No reuse allowed without permission.

against EHEC infection (56, 57). EspA, which was detected as the most abundant protein of LEE, forms a channel that connect the bacterial cytoplasm with the host cell; this exportation conduct allows the translocation of effectors from within the host cell (58). EspB together with EspD are responsible for the formation of the translocation pore and for the effector translocation of Tir (59). In addition, EspB can inhibit the interaction between myosin and actin, which promotes loss of microvilli and consequently contributes to the induction of diarrhea (60). The interaction between Tir and Intimin contributes directly to EHEC O157:H7 persistence during the infection process (61, 62). Furthermore, Tir and Intimin are involved in the modulation of host immunity. Tir might inhibit tumor necrosis factor receptor-associated factor 6 (TRAF6)-mediated by NF-κB activation (63). Instead, intimin can induce a T-helper cell type 1 response as well as to stimulate the proliferation of spleen CD4+ T lymphocytes and cells from lymphoid tissues (64, 65).

Conclusion

In this work, we applied the quantitative proteomic (TMT)-based and emPAI analyses to estimate the quantification of EHEC O157:H7 proteome of combined proteomes of two EHEC O157:H7 isolates from Argentinian cattle and of the standard strainEDL933. These comprehensive proteomic analyses generated a quantitative dataset of EHEC proteome composed of a subset of proteins involved in different biological processes. All these proteins together might form a network of factors that play an important role in the pathogenesis and physiology of this pathogen. Altogether, the results presented in this study provide insights into the functional genome of EHEC O157:H7 at the protein level

bioRxiv preprint doi: https://doi.org/10.1101/312652; this version posted May 2, 2018. The copyright holder for this preprint (which was not certified by peer review) is the author/funder. All rights reserved. No reuse allowed without permission.

and could contribute to the understating of the factors associated with the biology of this pathogen.

MATERIAL AND METHODS

Bacterial strain and growth conditions

The EHEC O157:H7 strains Rafaela II (clade 8) and 7.1 Anguil (clade 6) isolated from cattle in Argentina and EDL933 (clade 3) strain recovered from a patient in USA were routinely maintained in Luria-Bertani broth (LB, Difco Laboratories, USA) or in LB 1.5% bacteriological agar plates, at 37°C. For the proteomic studies, bacterial strains were cultured as previously described by Amigo et al. (7). Overnight cultures of the different EHEC O157:H7 strains growth in LB were inoculated (1:50) in Dulbecco's modified Eagle's medium (DMEM)-F12 nutrient until reach the mid-exponential growth phase ($OD_{600\ nm} = 0.6$) under a 5% CO_2 atmosphere at 37°C.

Protein extraction and preparation of whole bacterial lysates for LC-MS/MS

After bacterial growth, protein extractions were performed according to Amigo et al. (7). Three biological replicates of each culture were centrifuged at 5000 x g for 20 min at 4°C. The cell pellets were resuspended in ice-cold lysis buffer (50 mM Tris-HCl, pH 7.5, 25 mM NaCl, 5 mM DTT and 1 mM PMSF) and disrupted by three cycles in liquid N_2 and subsequently placed in boiling water. The resulting lysates were centrifuged at 30,000 × g for 10 min and precipitated with 5 volumes of ice-cold acetone at -20°C overnight. Next, the protein pellets were resuspended in buffer containing 8 M urea, 2 M thiocarbamide and 200 mM tetraethylammonium bromide at pH 8.5. The protein concentration was

bioRxiv preprint doi: https://doi.org/10.1101/312652; this version posted May 2, 2018. The copyright holder for this preprint (which was not certified by peer review) is the author/funder. All rights reserved. No reuse allowed without permission.

determined by the Bradford assay using BSA curve as a standard. Subsequently, the samples were reduced with tris-(2-carboxyethyl)-phosphine (200 mM), alkylated with iodoacetamide (375 mM) and enzymatically digested with sequencing grade trypsin. Finally, the samples were labeled with TMT Reagents 6-plex Kit according to the manufacturer's instructions.

Liquid chromatography and mass spectrometry

The proteomic analyses were performed using High pH Reverse Phase Fractionation and Nano LC-MS/MS Analysis by Orbitrap Fusion. Firstly, the labeled peptides were pooled together and desalted using Sep-Pak SPE (Waters) to remove salt ions. The hpRP chromatography was performed with Dionex UltiMate 3000 model on an Xterra MS C18 column (3.5 um, 2.1 × 150 mm, Waters). The sample were dissolved in buffer A (20 mM ammonium formate, pH 9.5) and then eluted with a gradient of 10 to 45% buffer B (80% acetonitrile (ACN)/20% 20 mM NH_4HCO_2) for 30 min, followed by 45% to 90% buffer B for 10 min, and a 5-min hold at 90% buffer B. Forty-eight fractions collected at 1 min intervals were merged into 12 fractions. The nano LC MS/MS analysis was carried out using a Orbitrap Fusion tribrid (Thermo-Fisher Scientific, San Jose, CA) mass spectrometer with an UltiMate 3000 RSLC nano system (Thermo-Dionex, Sunnyvale, CA). The fraction was injected onto a PepMap C18 trapping column (5 μm, 200 μm × 1 cm, Dionex) and separated on a PepMap C18 RP nano column (3 μm, 75 μm × 15 cm, Dionex).For all the analysis, the mass spectrometer was operated in positive ion mode, MS spectra were acquired across 350–1550 m/z scan mass range, at a resolution of 12,0000 in the Orbitrap with the max injection time of 50 ms. Tandem mass spectra were recorded in high

bioRxiv preprint doi: https://doi.org/10.1101/312652; this version posted May 2, 2018. The copyright holder for this preprint (which was not certified by peer review) is the author/funder. All rights reserved. No reuse allowed without permission.

sensitivity mode (resolution >30000) and made by HCD at normalized collision energy of 40. Each cycle of data-dependent acquisition (DDA) mode selected the top10 most intense peaks for fragmentation. The data were acquired with Xcalibur 2.1 software (Thermo-Fisher Scientific).

Database searching, Protein Identification and Abundance Estimation

Analyses were carried out by Mascot (version 2.4.1, Matrix Science, Boston, MA) against the databases described below. The raw files from MS/MS datasets were searched against a combined database of proteins composed by the annotation of EHEC O157:H7 TW14359 and EHEC O157:H7 EDL933 genomes. For protein identification, the parameters were used as follows: one missed cleavage was allowed with fixed carbamidomethylation (Cys), fixed 6-plex TMT modifications on Lys and N-terminal amines and variable modifications of oxidation (Met), deamidation (Asn and Gln). The peptide and fragment mass tolerance values were set as 8 ppm and 20 millimass units (mmu), respectively. The target-decoy strategy (66) and the Mascot-integrated percolator calculation were applied to estimate the false discovery rate (FDR). Only peptides above "identity" were counted as identified. Furthermore, a protein must produce at least two unique peptides that generate a complete TMT reporter ion series to be confidently quantified. MS/MS based peptide and protein identifications were validated via Scaffold (version Scaffold_4.4.3, Proteome Software Inc., Portland, OR).

Peptide identifications were accepted when the peptide FDR is below 1.0%. Protein identifications were accepted when the protein FDR is below 1.0% and at least two unique peptides could be quantified. The proteins that contained similar peptides and that could not

bioRxiv preprint doi: https://doi.org/10.1101/312652; this version posted May 2, 2018. The copyright holder for this preprint (which was not certified by peer review) is the author/funder. All rights reserved. No reuse allowed without permission.

be differentiated based on MS/MS analysis alone were grouped to satisfy the principles of parsimony. The intensities of reporter ions for each valid spectrum were normalized. The reference channels were normalized to produce a 1:1-fold change. All normalization calculations were performed using medians. The protein abundance index was obtained by emPAI analysis using protein identification data from Mascot and Scaffold and used to calculate the emPAI algorithm. The equation emPAI/Σ (emPAI) x 100 was used to calculate the protein content in mol%.

Bioinformatics analysis

Functional annotations were assigned by the COG database (14). Metabolic pathways were determined by analyzing proteins with the Kyoto Encyclopedia of Genes pathways and Genomes (KEGG) (19).

SUPPLEMENTAL MATERIAL

Supplemental File

ACKNOWLEDGMENTS

The present study was supported by grants PICT #0211 from FONCYT, Argentina, PNBIO1131034 INTA, Argentina; Presidential Foundation of Guangdong Academy of Agricultural Sciences (No.: 201320), and Science and Technology Program of Guangdong Province, (2016B070701013) China.

WMdS, AA, PV, ML and AC are CONICET fellows. NA holds a CONICET fellowship. We thank Julia Sabio y García for her critical reading.

bioRxiv preprint doi: https://doi.org/10.1101/312652; this version posted May 2, 2018. The copyright holder for this preprint (which was not certified by peer review) is the author/funder. All rights reserved. No reuse allowed without permission.

REFERENCES

[1] Noris M, Remuzzi G.2005. Hemolytic uremic syndrome. J Am SocNephrol 16:1035–1050.

[2] Scallan E, Hoekstra RM, Angulo FJ, Tauxe RV, Widdowson MA, Roy SL, Jones JL, Griffin PM. 2011. Foodborne illness acquired in the United States—major pathogens. Emerg Infect Dis 17:7–15.

[3] Ferraris JR, Ramirez JA, Ruiz S, Caletti MG, Vallejo G, Piantanida JJ, Araujo JL, Sojo ET. 2002. Shiga toxin-associated hemolytic uremic syndrome: absence of recurrence after renal transplantation. Ped Nephrol 17:809-814.

[4] Rivas M, Padola NL, Lucchesi PMA, Massana M. Diarrheagenic *Escherichia coli* in Argentina In: Torres AG, editor. Pathogenic*Escherichia coli* in Latin America. Oak Park (IL), EstadosUnidos: Bentham Science Publishers Ltd.; 2010. p. 142–61.

[5] Etcheverría AI1, Padola NL. 2013. Shiga toxin-producing *Escherichia coli*: factors involved in virulence and cattle colonization. Virulence 1:366-372.

[6] Amigo N, Mercado E, Bentancor A, Singh P, Vilte D, Gerhardt E, Zotta E, Ibarra C, Manning SD, Larzábal M, Cataldi A. 2015. Clade 8 and Clade 6 Strains of *Escherichia coli* O157:H7 from Cattle in Argentina have Hypervirulent-Like Phenotypes. PLoS One 10:e0127710.

[7] Amigo N, Zhang Q, Amadio A, Zhang Q, Silva WM, Cui B, Chen Z, Larzabal M, Bei J, Cataldi A. 2016. Overexpressed Proteins in Hypervirulent Clade 8 and Clade 6 Strains of *Escherichia coli* O157:H7 Compared to *E. coli* O157:H7 EDL933 Clade 3 Strain. PLoS One 23:e0166883.

bioRxiv preprint doi: https://doi.org/10.1101/312652; this version posted May 2, 2018. The copyright holder for this preprint (which was not certified by peer review) is the author/funder. All rights reserved. No reuse allowed without permission.

[8] Sadiq SM, Hazen TH, Rasko DA, Eppinger M. 2014. EHEC Genomics: Past, Present, and Future. Microbiol Spectr 2:EHEC-0020-2013.

[9] Bose T, Venkatesh KV, Mande SS. 2017. Computational Analysis of Host-Pathogen Protein Interactions between Humans and Different Strains of Enterohemorrhagic *Escherichia coli*. Front Cell Infect Microbiol 19:128.

[10] Otto A, Becher D, Schmidt F. 2014. Quantitative proteomics in the field of microbiology. Proteomics. 14:547-565.

[11] Otto A, Bernhardt J, Hecker M, Becher D. 2012. Global relative and absolute quantitation in microbial proteomics. Curr Opin Microbiol 15:364-372.

[12] Li H, Han J, Pan J, Liu T, Parker CE, Borchers CH. 2017. Current trends in quantitative proteomics - an update. J Mass Spectrom.52:319-341.

[13] Ishihama Y, Oda Y, Tabata T, Sato T, Nagasu T, Rappsilber J, Mann M. 2005. Exponentially modified protein abundance index (emPAI) for estimation of absolute protein amount in proteomics by the number of sequenced peptides per protein. Mol Cell Proteomics 4:1265-1272.

[14] Galperin MY, Makarova KS, Wolf YI, Koonin EV. 2015. Expanded microbial genome coverage and improved protein family annotation in the COG database. Nucleic Acids Res. 43:D261-9.

[15] Pieper R, Zhang Q, Clark DJ, Huang ST, Suh MJ, Braisted JC, Payne SH, Fleischmann RD, Peterson SN, Tzipori S. 2011. Characterizing the *Escherichia coli* O157:H7 Proteome Including Protein Associations with Higher Order Assemblies. PLoS One 6:e26554.

bioRxiv preprint doi: https://doi.org/10.1101/312652; this version posted May 2, 2018. The copyright holder for this preprint (which was not certified by peer review) is the author/funder. All rights reserved. No reuse allowed without permission.

419 [16] Ishihama Y, Schmidt T, Rappsilber J, Mann M, Hartl FU, Kerner MJ, Frishman D.
420 2008. Protein abundance profiling of the *Escherichia coli* cytosol. BMC Genomics
421 27:102.
422 [17] Harris SM, Yue WF, Olsen SA, Hu J, Means WJ, McCormick RJ, Du M, Zhu MJ.
423 2012. Salt at concentrations relevant to meat processing enhances Shiga toxin 2
424 production in *Escherichia coli* O157:H7. Int J Food Microbiol 15:186-192.
425 [18] Mei GY, Tang J, Carey C, Bach S, Kostrzynska M. 2015. The effect of oxidative
426 stress on gene expression of Shiga toxin-producing *Escherichia coli* (STEC)
427 O157:H7 and non-O157 serotypes. Int J Food Microbiol 23:7-15.
428 [19] Kanehisa M, Goto S, Sato Y, Furumichi M, Tanabe M. 2012. KEGG for integration
429 and interpretation of large-scale molecular data sets. Nucleic Acids Res 40: D109–
430 D114.
431 [20] Miranda RL, Conway T, Leatham MP, Chang DE, Norris WE, Allen JH, Stevenson
432 SJ, Laux DC, Cohen PS. 2004. Glycolytic and gluconeogenic growth of *Escherichia*
433 *coli* O157:H7 (EDL933) and *E. coli* K-12 (MG1655) in the mouse intestine. Infect
434 Immun 72:1666-1676.
435 [21] Bertin Y, Deval C, de la Foye A, Masson L, Gannon V, Harel J, Martin C, Desvaux
436 M, Forano E. 2014. The gluconeogenesis pathway is involved in maintenance of
437 enterohaemorrhagic *Escherichia coli* O157:H7 in bovine intestinal content. PLoS
438 One 2:e98367.
439 [22] Njoroge JW, Nguyen Y, Curtis MM, Moreira CG, Sperandio V. 2012. Virulence
440 meets metabolism: Cra and KdpE gene regulation in enterohemorrhagic *Escherichia*
441 *coli*. MBio 16:e00280-12.

bioRxiv preprint doi: https://doi.org/10.1101/312652; this version posted May 2, 2018. The copyright holder for this preprint (which was not certified by peer review) is the author/funder. All rights reserved. No reuse allowed without permission.

442 [23] Henderson B, Martin AC. 2014. Protein moonlighting: a new factor in biology and
443 medicine. Biochem Soc Trans 42:1671-1678.

444 [24] Egea L, Aguilera L, Giménez R, Sorolla MA, Aguilar J, Badía J, Baldoma L. 2007.
445 Role of secreted glyceraldehyde-3-phosphate dehydrogenase in the infection
446 mechanism of enterohemorrhagic and enteropathogenic *Escherichia coli*: interaction
447 of the extracellular enzyme with human plasminogen and fibrinogen. Int J Biochem
448 Cell Biol 39:1190-1203.

449 [25] Aguilera L, Giménez R, Badia J, Aguilar J, Baldoma L. 2009. NAD+-dependent post-
450 translational modification of *Escherichia coli* glyceraldehyde-3-phosphate
451 dehydrogenase. Int Microbiol 12:187-192.

452 [26] Murashko ON, Lin-Chao S. 2017. *Escherichia coli* responds to environmental
453 changes using enolasicdegradosomes and stabilized DicF sRNA to alter cellular
454 morphology. Proc Natl Acad Sci U S A 19:E8025-E8034.

455 [27] Gingold H, and Pilpel Y. 2011. Determinants of translation efficiency and accuracy.
456 Mol Syst Biol 12:481.

457 [28] Alpert C, Scheel J, Engst W, Loh G, Blaut M. 2009. Adaptation of protein expression
458 by *Escherichia coli* in the gastrointestinal tract of gnotobiotic mice. Environ
459 Microbiol 11:751-761.

460 [29] Ribeiro CB, Sobral MG, Tanaka CL, Dallagassa CB, Picheth G, Rego FG, Alberton
461 D, Huergo LF, Pedrosa FO, Souza EM, Fadel-Picheth CM. 2013. Proteins
462 differentially expressed by Shiga toxin-producing *Escherichia coli* strain M03 due to
463 the biliar salt sodium deoxycholate. Genet Mol Res 24:4909-4917.

bioRxiv preprint doi: https://doi.org/10.1101/312652; this version posted May 2, 2018. The copyright holder for this preprint (which was not certified by peer review) is the author/funder. All rights reserved. No reuse allowed without permission.

464 [30] Jiang W, Hou Y, Inouye M. 1997. CspA, the major cold-shock protein of *Escherichia*
465 *coli*, is an RNA chaperone. J Biol Chem 3:196-202.
466 [31] Kakkanat A, Phan MD, Lo AW, Beatson SA, Schembri MA. 2017. Novel genes
467 associated with enhanced motility of *Escherichia coli* ST131. PLoS One
468 10:e0176290.
469 [32] Fratamico PM, DebRoy C, Liu Y, Needleman DS, Baranzoni GM, Feng P. 2016.
470 Advances in Molecular Serotyping and Subtyping of *Escherichia coli*. Front
471 Microbiol. 3:644.
472 [33] Zhou X, Girón JA, Torres AG, Crawford JA, Negrete E, Vogel SN, Kaper JB. 2003.
473 Flagellin of enteropathogenic *Escherichia coli* stimulates interleukin-8 production in
474 T84 cells. Infect Immun 71:2120-2129.

475 [34] Carruthers MD, Minion C. 2009. Transcriptome analysis of *Escherichia coli*
476 O157:H7 EDL933 during heat shock. FEMS Microbiol Lett 295:96-102.
477 [35] Singh R, Jiang X. 2015. Expression of stress and virulence genes in *Escherichia coli*
478 O157:H7 heat shocked in fresh dairy compost. J Food Prot 78:31-41.
479 [36] Kudva IT, Stanton TB, Lippolis JD. 2014. The *Escherichia coli* O157:H7 bovine
480 rumen fluid proteome reflects adaptive bacterial responses. BMC Microbiol 21;14:48.
481 [37] Vidovic S, Korber DR. 2016. *Escherichia coli* O157: Insights into the adaptive stress
482 physiology and the influence of stressors on epidemiology and ecology of this human
483 pathogen. Crit Rev Microbiol 42:83-93.
484 [38] Cha MK, Kim HK, Kim IH. 1996. Mutation and Mutagenesis of thiol peroxidase of
485 *Escherichia coli* and a new type of thiol peroxidase family. J Bacteriol 178:5610-
486 5614.

bioRxiv preprint doi: https://doi.org/10.1101/312652; this version posted May 2, 2018. The copyright holder for this preprint (which was not certified by peer review) is the author/funder. All rights reserved. No reuse allowed without permission.

487 [39] Seaver LC, Imlay JA. 2001. Alkyl hydroperoxide reductase is the primary scavenger
488 of endogenous hydrogen peroxide in *Escherichia coli*. J Bacteriol 183:7173-7181.
489 [40] Meyer Y, Buchanan BB, Vignols F, Reichheld JP. 2009. Thioredoxins and
490 glutaredoxins: unifying elements in redox biology. Annu Rev Gene 43:335-367.
491 [41] Smirnova G, Muzyka N, Lepekhina E, Oktyabrsky O. 2016. Roles of the glutathione-
492 and thioredoxin-dependent systems in the *Escherichia coli* responses to ciprofloxacin
493 and ampicillin. Arch Microbiol 198:913-921.
494 [42] Taylor DE. 1999. Bacterial tellurite resistance. Trends Microbiol 7:111-115.
495 [43] Kormutakova R, Klucar L, Turna J. 2000. DNA sequence analysis of the tellurite-
496 resistance determinant from clinical strain of *Escherichia coli* and identification of
497 essential genes. Biometals 13:135-159.
498 [44] Valkova D, Valkovicova L, Vavrova S, Kovacova E, Mravec J, Turna J. 2007. The
499 contribution of tellurite resistance genes to the fitness of *Escherichia coli*
500 uropathogenic strains. Cent Eur J Biol 2:182–191.
501 [45] Yin X, Wheatcroft R, Chambers JR, Liu B, Zhu J, Gyles CL 2009. Contributions of
502 O island 48 to adherence of enterohemorrhagic *Escherichia coli* O157:H7 to
503 epithelial cells in vitro and in ligated pig ileal loops. Appl Environ Microbiol
504 75:5779-5786
505 [46] Kudva IT, Griffin RW, Krastins B, Sarracino DA, Calderwood SB, John M. 2012.
506 Proteins other than the locus of enterocyte effacement-encoded proteins contribute to
507 *Escherichia coli* O157:H7 adherence to bovine rectoanal junction stratified squamous
508 epithelial cells. BMC Microbiol 12:103.

bioRxiv preprint doi: https://doi.org/10.1101/312652; this version posted May 2, 2018. The copyright holder for this preprint (which was not certified by peer review) is the author/funder. All rights reserved. No reuse allowed without permission.

509 [47] Islam N, Nagy A, Garrett WM, Shelton D, Cooper B, Nou X. 2016. Different
510 Cellular Origins and Functions of Extracellular Proteins from *Escherichia coli*
511 O157:H7 and O104:H4 as Determined by Comparative Proteomic Analysis. Appl
512 Environ Microbio l30:4371-4378.
513 [48] Kalule JB, Fortuin S, Calder B, Robberts L, Keddy KH, Nel AJM, Garnett S, Nicol
514 M, Warner DF, Soares NC, Blackburn JM. 2017. Proteomic comparison of three
515 clinical diarrhoeagenic drug-resistant *Escherichia coli* isolates grown on
516 CHROMagar™STEC media. J Proteomics 5: S1874-3919.
517 [49] Kim Y, Oh S, Ahn EY, Imm JY, Oh S, Park S, Kim SH. 2007. Proteome Analysis of
518 Virulence Factor Regulated by Autoinducer-2–like Activity in *Escherichia coli*
519 O157:H7 J Food Prot70:300-307.
520 [50] Elliott SJ, Wainwright LA, McDaniel TK, Jarvis KG, Deng YK, Lai LC, McNamara
521 BP, Donnenberg MS, Kaper JB. 1998. The complete sequence of the locus of
522 enterocyte effacement (LEE) from enteropathogenic Escherichia coli E2348/69. Mol
523 Microbiol 28:1-4.
524 [51] Russell RM, Sharp FC, Rasko DA, Sperandio V. 2007. QseA and GrlR/GrlA
525 regulation of the locus of enterocyte effacement genes in enterohemorrhagic
526 Escherichia coli. J Bacteriol 189:5387-5392.
527 [52] Stevens MP, Frankel GM. 2014. The Locus of Enterocyte Effacement and Associated
528 Virulence Factors of Enterohemorrhagic *Escherichia coli*. MicrobiolSpectr 2:EHEC-
529 0007-2013.
530 [53] Tobe T, Beatson SA, Taniguchi H, Abe H, Bailey CM, Fivian A, Younis R,
531 Matthews S, Marches O, Frankel G, Hayashi T, Pallen MJ. 2006. An extensive

bioRxiv preprint doi: https://doi.org/10.1101/312652; this version posted May 2, 2018. The copyright holder for this preprint (which was not certified by peer review) is the author/funder. All rights reserved. No reuse allowed without permission.

repertoire of type III secretion effectors in *Escherichia coli* O157 and the role of lambdoid phages in their dissemination. Proc Natl Acad Sci U S A 3:14941-14946.

[54] Naylor SW, Roe AJ, Nart P, Spears K, Smith DG, Low JC, Gally DL. 2005. *Escherichia coli* O157: H7 forms attaching and effacing lesions at the terminal rectum of cattle and colonization requires the LEE4 operon. Microbiology 151:2773-2781.

[55] Sharma VK, Kudva IT, Bearson BL, Stasko JA. 2016. Contributions of EspA Filaments and Curli Fimbriae in Cellular Adherence and Biofilm Formation of Enterohemorrhagic *Escherichia coli* O157:H7. PLoS One 22:e0149745.

[56] Li Y, Frey E, Mackenzie AM, Finlay BB. 2000. Human response to *Escherichia coli* O157:H7 infection: antibodies to secreted virulence factors. Infect Immun 68:5090-5095.

[57] Vilte DA, Larzábal M, Garbaccio S, Gammella M, Rabinovitz BC, Elizondo AM, Cantet RJ, Delgado F, Meikle V, Cataldi A, Mercado EC. 2011. Reduced faecal shedding of *Escherichia coli* O157:H7 in cattle following systemic vaccination with γ-intimin C_{280} and EspB proteins. Vaccine. 23:3962-3968.

[58] Ebel F, Podzadel T, Rohde M, Kresse AU, Krämer S, Deibel C, Guzmán CA, Chakraborty T. 1998. Initial binding of Shiga toxin-producing *Escherichia coli* to host cells and subsequent induction of actin rearrangements depend on filamentous EspA-containing surface appendages. Mol Microbiol 30:147-161.

[59] Hartland EL, Daniell SJ, Delahay RM, Neves BC, Wallis T, Shaw RK, Hale C, Knutton S, Frankel G. 2000. The type III protein translocation system of

bioRxiv preprint doi: https://doi.org/10.1101/312652; this version posted May 2, 2018. The copyright holder for this preprint (which was not certified by peer review) is the author/funder. All rights reserved. No reuse allowed without permission.

554 enteropathogenic Escherichia coli involves EspA-EspB protein interactions. Mol
555 Microbiol 35:1483–1492.

556 [60] Iizumi Y, Sagara H, Kabe Y, Azuma M, Kume K, Ogawa M, Nagai T, Gillespie PG,
557 Sasakawa C, Handa H. 2007. The enteropathogenic *E. coli* effector EspB facilitates
558 microvillus effacing and antiphagocytosis by inhibiting myosin function. Cell Host
559 Microbe Dec 13:383-392.

560 [61] Cornick NA, Booher SL, Moon HW. 2002. Intimin facilitates colonization
561 by *Escherichia coli* O157:H7 in adult ruminants.Infect Immun 70:2704–2707.

562 [62] Dean-Nystrom EA, Bosworth BT, Moon HW, O'Brien AD.1998.*Escherichia coli*
563 O157:H7 requires intimin for enteropathogenicity in calves. Infect Immun 66:4560–
564 4563.

565 [63] Yan D, Quan H, Wang L, Liu F, Liu H, Chen J, Cao X, Ge B. 2013.
566 Enteropathogenic *Escherichia coli* Tir recruits cellular SHP-2 through ITIM motifs to
567 suppress host immune response. Cell Signal 25:1887-1894.

568 [64] Higgins LM, Frankel G, Connerton I, Gonçalves NS, Dougan G, MacDonald TT.
569 1999. Role of bacterial intimin in colonic hyperplasia and inflammation. Science
570 285:588–591.

571 [65] Gonçalves NS, Hale C, Dougan G, Frankel G, MacDonald TT. 2003. Binding of
572 intimin from enteropathogenic Escherichia coli to lymphocytes and its functional
573 consequences. Infect Immun 71:2960–2965.

574 [66] Elias JE, Gygi SP. 2010. Target-decoy search strategy for mass spectrometry-based
575 proteomics. Methods Mol Biol 604:55–71.

bioRxiv preprint doi: https://doi.org/10.1101/312652; this version posted May 2, 2018. The copyright holder for this preprint (which was not certified by peer review) is the author/funder. All rights reserved. No reuse allowed without permission.

Figure legend

Figure 1: Characterization of EHEC O157:H7 proteome and correlation with *in silico* data. **(A)** Distribution of the peptides detected by MS. **(B)** Correlation of the proteomic results with *in silico* data of EHEC O157:H7 genome. **(C)** Dynamic range based on the emPAI value of the proteins identified by LC-MS analysis; pink, most abundant proteins; green, less abundant proteins and red, proteins that are present in the LEE pathogenicity island.

Figure 2: Functional analysis of the EHEC O157:H7 proteome.(A) Proteins classified by COG functional categories **(B)** Categorization of the proteins identified into biological processes. [E] Amino acid transport and metabolism; [G] carbohydrate transport and metabolism; [D] cell cycle control, cell division, and chromosome partitioning; [N] cell motility; [M] cell wall/membrane/envelope biogenesis; [H] coenzyme transport and metabolism; [V] defense mechanisms; [C] energy production and conversion; [W] extracellular structures; [S] function unknown; [R] general function prediction only; [P] inorganic ion transport and metabolism; [U] intracellular trafficking, secretion, and vesicular transport; [I] lipid transport and metabolism; [X] mobilome: prophages, transposons; [F] nucleotide transportand metabolism; [O] post-translational modification, protein turnover and chaperones; [L] replication, recombination, and repair; [A] RNA processing and modification; [Q] secondary metabolite biosynthesis, transport, and catabolism; [T] signal transduction mechanisms; [K] transcription; [J] translation, ribosomal structure and biogenesis. **(C)** KEGG pathway enrichment analysis, the colors are based on the protein abundance; blue, most abundant and green, less abundant.

bioRxiv preprint doi: https://doi.org/10.1101/312652; this version posted May 2, 2018. The copyright holder for this preprint (which was not certified by peer review) is the author/funder. All rights reserved. No reuse allowed without permission.

598 **Figure 3: Overview of the Glycolysis / Gluconeogenesis pathway of EHEC**
599 **O157:H7.**Enzymes of the Glycolysis / Gluconeogenesis metabolism that were identified at
600 the proteome level. Blue, proteins detected in our proteomic analysis; Green, proteins not
601 identified in our study and Red, proteins detected as most abundant.

bioRxiv preprint doi: https://doi.org/10.1101/312652; this version posted May 2, 2018. The copyright holder for this preprint (which was not certified by peer review) is the author/funder. All rights reserved. No reuse allowed without permission.

Table 1: List of the most abundant proteins of EHEC O157:H7 proteome

Access Number	Description	Protein content (mol %)	COGSymbol[(a)]
gi|667692306	NAD-dependent glyceraldehyde-3-phosphate dehydrogenase	3,71	G
gi|667694059	SSU ribosomal protein S5p (S2e)	3,55	J
gi|667692489	Flagellar biosynthesis protein FliC	3,38	N
gi|667693503	Enolase	3,27	G
gi|667693720	putative Fe(2+)-trafficking protein YggX	3,17	PO
gi|667693013	Hypothetical protein	3,09	S
gi|667695021	Heat shock protein 60 family chaperone GroEL	3,08	O
gi|667689612	Chaperone protein DnaK	3,04	O
gi|667690667	Tellurium resistance protein TerD	3,00	T
gi|667693130	Phosphotransferase system, phosphocarrier protein	2,85	TG
gi|667694476	EspA	2,82	J
gi|667694778	Triosephosphate isomerase	2,79	G
gi|667691933	Thiol peroxidase, Tpx-type	2,78	O
gi|667692763	DNA-damage-inducible protein I	2,78	P
gi|667694337	Dipeptide-binding ABC transporter	2,76	E
gi|667690668	Tellurium resistance protein TerE	2,75	T
gi|667694081	Translation elongation factor Tu	2,69	J
gi|667690420	Phosphoglycerate mutase	2,68	G
gi|667693674	Phosphoglycerate kinase	2,65	G
gi|667691384	Isocitrate dehydrogenase [NADP]	2,64	C
gi|667689773	Translation elongation factor Ts	2,63	J
gi|667695123	Endoribonuclease L-PSP	2,62	V
gi|667691519	DNA-binding protein H-NS	2,61	K
gi|667691364	Hypothetical protein	2,59	I
gi|667691726	Glutamate decarboxylase	2,56	E
gi|667690418	putative secreted protein	2,56	S
gi|667694844	LSU ribosomal protein L1p (L10Ae)	2,54	J
gi|667694305	Glutamate decarboxylase	2,52	E
gi|667695075	SSU ribosomal protein S6p	2,47	J
gi|667690270	Alkyl hydroperoxidereductase protein C	2,46	V
gi|667695256	Purine nucleoside phosphorylase	2,45	F
gi|667689607	Transaldolase	2,43	G
gi|667695020	Heat shock protein 60 family co-chaperone GroES	2,43	O
gi|667694296	Chaperone HdeA	2,42	C
gi|667694705	Periplasmic thiol:disulfide interchange protein	2,41	O

bioRxiv preprint doi: https://doi.org/10.1101/312652; this version posted May 2, 2018. The copyright holder for this preprint (which was not certified by peer review) is the author/funder. All rights reserved. No reuse allowed without permission.

gi|667690756	Phosphoserine aminotransferase	2,39	HE
gi|667694406	Glutaredoxin 3 (Grx3)	2,39	O
gi|667692485	Cystine ABC transporter	2,38	ET
gi|667692357	Cold shock protein CspA	2,37	K
gi|667694062	SSU ribosomal protein S8p (S15Ae)	2,34	J
gi|667694071	LSU ribosomal protein L22p (L17e)	2,33	J
gi|667695077	LSU ribosomal protein L9p	2,32	J
gi|667691029	Ferrous iron transport periplasmic protein	2,29	C
gi|667691774	Hypothetical protein	2,29	R
gi|667694592	ATP synthase beta chain	2,29	C
gi|667694268	Universal stress protein A	2,29	T
gi|667690733	Translation initiation factor 1	2,27	J
gi|667694868	IMP cyclohydrolase	2,27	F
gi|667694766	Manganese superoxide dismutase	2,26	P
gi|667690203	Peptidyl-prolyl cis-trans isomerase PpiB	2,25	O
gi|667694064	LSU ribosomal protein L5p (L11e)	2,25	J
gi|667690810	Outer membrane protein A precursor	2,24	M
gi|667691522	Alcohol dehydrogenase	2,24	C
gi|667693128	Cysteine synthase	2,24	E
gi|667690777	Aspartate aminotransferase	2,24	E
gi|667694846	LSU ribosomal protein L7/L12 (P1/P2)	2,23	J
gi|667690752	Pyruvate formate-lyase	2,23	C
gi|667693266	Serine hydroxymethyltransferase	2,22	E
gi|667691738	Osmotically inducible protein C	2,21	V
gi|667689716	Dihydrolipoamide acetyltransferase	2,20	C
gi|667693332	DNA-damage-inducible protein I	2,19	OT
gi|667689715	Pyruvate dehydrogenase E1 component	2,16	C
gi|667690091	hypothetical protein YajQ	2,16	S
gi|667690760	SSU ribosomal protein S1p	2,15	K
gi|667694072	SSU ribosomal protein S19p (S15e)	2,14	J
gi|667692196	Pyruvate kinase	2,14	G
gi|667691439	Protease VII (Omptin) precursor	2,14	M
gi|667693243	Iron-sulfur cluster assembly scaffold protein IscU	2,13	O
gi|667692658	6-phosphogluconate dehydrogenase, decarboxylating	2,12	G
gi|667693132	PTS system, glucose-specific IIA component	2,11	G
gi|667694683	Uridine phosphorylase	2,11	F
gi|667689775	Ribosome recycling factor	2,11	J
gi|667690429	Molybdenum ABC transporter	2,10	P
gi|667694065	LSU ribosomal protein L24p (L26e)	2,10	J
gi|667689933	Hypothetical protein	2,08	F
gi|667694594	Peptidyl-prolylcis-trans isomerasePpiA precursor	2,07	C
gi|667694106	ATP synthase alpha chain	2,07	O

bioRxiv preprint doi: https://doi.org/10.1101/312652; this version posted May 2, 2018. The copyright holder for this preprint (which was not certified by peer review) is the author/funder. All rights reserved. No reuse allowed without permission.

gi|667690289	Cold shock protein CspA	2,06	K
gi|667695103	Inorganic pyrophosphatase	2,06	CP
gi|667694625	Ketol-acid reductoisomerase	2,06	EH
gi|667694890	Glucose-6-phosphate isomerase	2,05	G
gi|667690141	hypothetical protein co-occurring with RecR	2,03	R
gi|667694076	LSU ribosomal protein L3p (L3e)	2,03	J
gi|667693201	Arsenate reductase	2,03	P
gi|667694068	LSU ribosomal protein L29p (L35e)	2,01	J

(a) COG groups are defined in the legend to Fig. 2B.

2

bioRxiv preprint doi: https://doi.org/10.1101/312652; this version posted May 2, 2018. The copyright holder for this preprint (which was not certified by peer review) is the author/funder. All rights reserved. No reuse allowed without permission.

Table 2: List of the most abundant proteins detected in *E. coli* K-12 and EHEC 86-24

Access Number	Gene name	Description	Detection	
			***E. coli* K-12**	**EHEC 86-24**
gi|667692306	*gapA*	Glyceraldehyde-3-phosphate dehydrogenase	M	M
gi|667694081	*tuf*	Translation elongation factor Tu	M	M
gi|667691519	*hns*	DNA-binding protein H-NS	M	M
gi|667690270	*ahpC*	Alkyl hydroperoxidereductase protein C	M	M
gi|667694846	*rplL*	50S ribosomal protein L7/L12 (P1/P2)	M	M
gi|667695021	*groEL*	Heat shock protein 60 family chaperone GroEL	M	M
gi|667694059	*rpsE*	30S ribosomal protein S5		M
gi|667691933	*tpx*	Thiol peroxidase, Tpx-type		M
gi|667691384	*icdA*	Isocitrate dehydrogenase [NADP]		M
gi|667695020	*groES*	Heat shock protein 60 family co-chaperone GroES		M
gi|667694592	*atpD*	ATP synthase beta chain		M
gi|667690810	*ompA*	Outer membrane protein A		M
gi|667693130	*ptsH*	Phosphotransferase system, phosphocarrier protein HPr	M	
gi|667693674	*pgk*	Phosphoglycerate kinase	M	
gi|667689773	*tsf*	Translation elongation factor Ts	M	
gi|667694844	*rplA*	50S ribosomal protein L1	M	
gi|667694071	*rplV*	50S ribosomal protein L22	M	
gi|667690760	*rpsA*	30S ribosomal protein S1	M	
gi|667694072	*rpsS*	SSU ribosomal protein S19p (S15e)	M	
gi|667693132	*crr*	PTS system, glucose-specific IIA component	M	
gi|667694065	*rplX*	LSU ribosomal protein L24p (L26e)	M	
gi|667694076	*rplC*	LSU ribosomal protein L3p (L3e)	M	
gi|667694068	*rpmC*	LSU ribosomal protein L29p (L35e)	M	

All proteins were detected in the proteomic study of E. coli K-12 (Ishihama et al., 2008) and EHEC 86-24 (Pieper et al., 2011).

M = proteins detected at high levels

1

bioRxiv preprint doi: https://doi.org/10.1101/312652; this version posted May 2, 2018. The copyright holder for this preprint (which was not certified by peer review) is the author/funder. All rights reserved. No reuse allowed without permission.

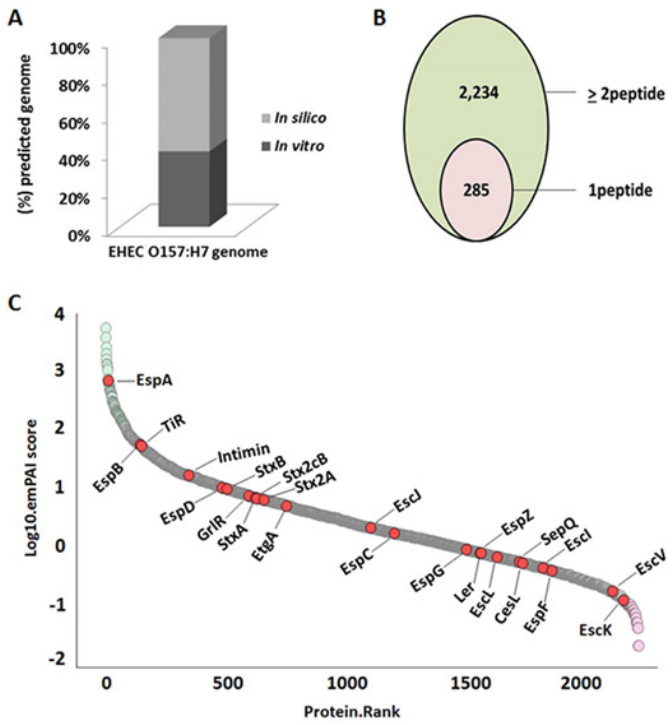

Figure 3: Overview of the Glycolysis / Gluconeogenesis pathway of EHEC O157:H7. Enzymes of the Glycolysis / Gluconeogenesis metabolism that were identified at the proteome level. Blue, proteins detected in our proteomic analysis; Green, proteins not identified in our study and Red, proteins detected as most abundant.

bioRxiv preprint doi: https://doi.org/10.1101/312652; this version posted May 2, 2018. The copyright holder for this preprint (which was not certified by peer review) is the author/funder. All rights reserved. No reuse allowed without permission.

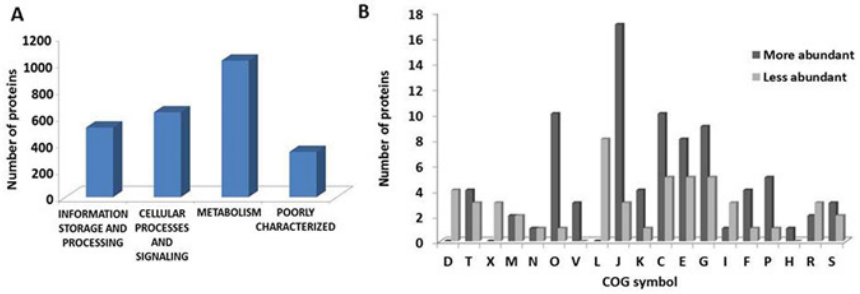

C

KEEG Pathway	P-Value	Corrected P-Value
Glycolysis / Gluconeogenesis	9,71E-10	8,79E-08
Carbon metabolism	1,78E-09	8,79E-08
Ribosome	3,37E-09	1,11E-07
Biosynthesis of antibiotics	5,20E-09	1,29E-07
Biosynthesis of secondary metabolites	7,18E-08	1,42E-06
Biosynthesis of amino acids	2,93E-07	3,63E-06
Microbial metabolism in diverse environments	3,48E-07	3,83E-06
Metabolic pathways	1,78E-04	1,26E-03
Methane metabolism	1,90E-03	1,26E-02
Pyruvate metabolism	2,74E-03	1,59E-02
RNA degradation	4,07E-03	2,24E-02
Butanoate metabolism	5,36E-03	2,80E-02
Taurine and hypotaurine metabolism	7,89E-03	3,60E-02
Homologous recombination	4,72E-05	2,27E-03

Figure 2: Functional analysis of the EHEC O157:H7 proteome.(A) Proteins classified by COG functional categories **(B)** Categorization of the proteins identified into biological processes. [E] Amino acid transport and metabolism; [G] carbohydrate transport and metabolism; [D] cell cycle control, cell division, and chromosome partitioning; [N] cell motility; [M] cell wall/membrane/envelope biogenesis; [H] coenzyme transport and metabolism; [V] defense mechanisms; [C] energy production and conversion; [W] extracellular structures; [S] function unknown; [R] general function prediction only; [P] inorganic ion transport and metabolism; [U] intracellular trafficking, secretion, and vesicular transport; [I] lipid transport and metabolism; [X] mobilome: prophages, transposons; [F] nucleotide transportand metabolism; [O] post-translational modification, protein turnover and chaperones; [L] replication, recombination, and repair; [A] RNA processing and modification; [Q] secondary metabolite biosynthesis, transport, and catabolism; [T] signal transduction mechanisms; [K] transcription; [J] translation, ribosomal structure and biogenesis. **(C)** KEGG pathway enrichment analysis, the colors are based on the protein abundance; blue, most abundant and green, less abundant.

bioRxiv preprint doi: https://doi.org/10.1101/312652; this version posted May 2, 2018. The copyright holder for this preprint (which was not certified by peer review) is the author/funder. All rights reserved. No reuse allowed without permission.

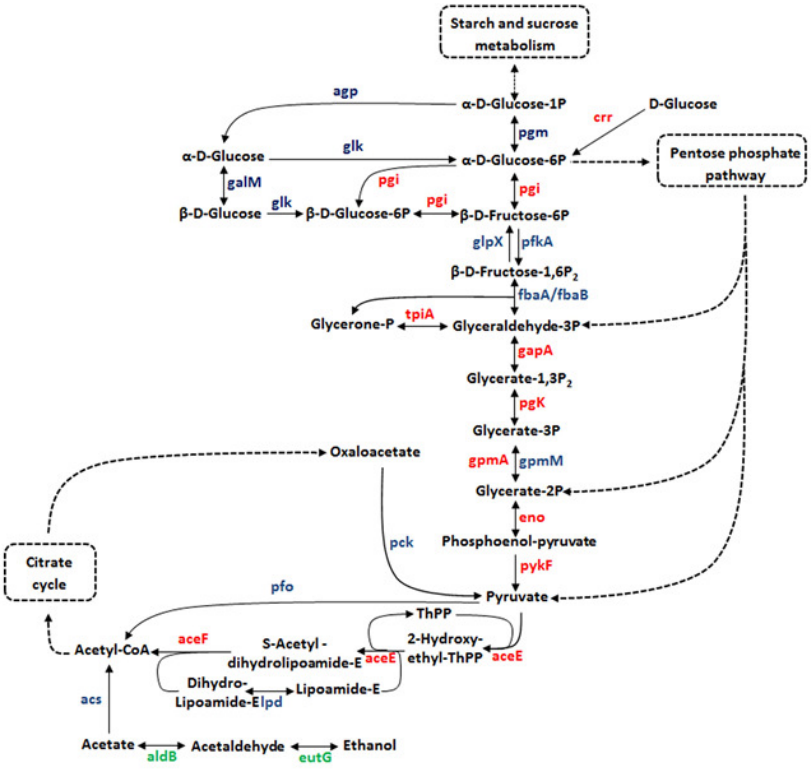

Figure 1: Characterization of EHEC O157:H7 proteome and correlation with *in silico* data. **(A)** Distribution of the peptides detected by MS. **(B)** Correlation of the proteomic results with *in silico* data of EHEC O157:H7 genome. **(C)** Dynamic range based on the emPAI value of the proteins identified by LC-MS analysis; pink, most abundant proteins; green, less abundant proteins and red, proteins that are present in the LEE pathogenicity island